Elastic, mechanical, and thermodynamic properties of Bi-Sb binaries: Effect of spin-orbit coupling

Sobhit Singh,[1,*] Irais Valencia-Jaime,[2] Olivia Pavlic,[1] and Aldo H. Romero[1]
[1]*Department of Physics and Astronomy, West Virginia University, Morgantown, West Virginia 26505-6315, USA*
[2]*Department of Chemistry, University of North Dakota, Grand Forks, North Dakota 58202, USA*

(Received 30 November 2017; published 20 February 2018)

Using first-principles calculations, we systematically study the elastic stiffness constants, mechanical properties, elastic wave velocities, Debye temperature, melting temperature, and specific heat of several thermodynamically stable crystal structures of Bi_xSb_{1-x} ($0 < x < 1$) binaries, which are of great interest due to their numerous inherent rich properties, such as thermoelectricity, thermomagnetic cooling, strong spin-orbit coupling (SOC) effects, and topological features in the electronic band structure. We analyze the bulk modulus (B), Young's modulus (E), shear modulus (G), B/G ratio, and Poisson's ratio (ν) as a function of the Bi concentration in Bi_xSb_{1-x}. The effect of SOC on the above-mentioned properties is further investigated. In general, we observe that the SOC effects cause elastic softening in most of the studied structures. Three monoclinic structures of Bi-Sb binaries are found to exhibit significantly large auxetic behavior due to the hingelike geometric structure of bonds. The Debye temperature and the magnitude of the elastic wave velocities monotonically increase with increasing Sb concentration. However, anomalies were observed at very low Sb concentration. We also discuss the specific-heat capacity versus temperature data for all studied binaries. Our theoretical results are in excellent agreement with the existing experimental and theoretical data. The comprehensive understanding of the material properties such as hardness, mechanical strength, melting temperature, propagation of the elastic waves, auxeticity, and heat capacity is vital for practical applications of the studied binaries.

DOI: 10.1103/PhysRevB.97.054108

I. INTRODUCTION

A thorough understanding of the mechanical response of any given material is essential before the technological applications of that particular material can be realized. A good place to start is investigating the elasticity, a fundamental property of a crystal which governs the macroscopic response of the crystal under external forces. The hardness, mechanical strength, and the propagation of the sound and elastic waves in a given material can be determined by knowledge of the elastic constants of that particular material. Among many known binary compounds and alloys, Bi-Sb-based binaries have retained a peculiar place due to their applications in the low-temperature thermoelectric industry and refrigeration [1–5]. Moreover, Bi-Sb binaries are the first predicted three-dimensional topological insulator (often referred as the first-generation topological insulator) that hosts robust conducting surface states [6–10]. Soon after the theoretical prediction, Hseih *et al.* [7] reported the experimental detection of novel gapless conducting surface states in this binary system. Recently, we found that the lowest-energy structure of BiSb composition (in $R3m$ space group) exhibits large ferroelectric behavior along with a giant tunable Rashba-Dresselhaus effect, which is the result of the broken inversion symmetry and the large spin-orbit coupling (SOC) of the constituent Bi and Sb elements [11,12]. Furthermore, we demonstrated that one can realize a Weyl semimetallic phase under external stress of 4–6 GPa [11]. Interestingly, by exploiting an interlink between the large SOC of the constituent atoms and the ferroelectric polarization, one can tune the dynamics of Weyl fermions in the momentum space of BiSb. This particular property is of notable interest for applications of Weyl semimetals in the forthcoming Weyltronic technology.

BiSb is not only interesting in its bulk phase, but it also shows unique electronic properties in two dimensions [13–16]. In particular, a giant tunable Rashba effect along with a large direct band gap (∼1.6 eV) have been reported for this system [16]. The existence of the large tunable Rashba effect together with a direct band gap in the visible region makes this material of particular interest for its applications in the optoelectronics and spintronics industry. Recently, Yu *et al.* [14] investigated the topological properties of monolayer BiSb and observed the emergence of a robust novel quantum spin Hall (QSH) effect under biaxial tensile strain. This finding was further confirmed by the calculation of the Z2 topological invariant and the nontrivial topological edge states. These features make BiSb an attractive candidate for applications in spintronic devices.

Other than the BiSb composition, several other stable compositions of the Bi-Sb binaries have been reported in the literature in both theoretical and experimental studies [1–3,5,12,17–20]. The formation mechanism and the chemical synthesis procedure of Bi_xSb_{1-x} nanocrystals are given in Refs. [21–23]. A detailed structural, electronic, vibrational, and thermoelectric investigation of the Bi-Sb binaries can be found in our recent work [12]. In Ref. [12], we explored the potential-energy surface of Bi-Sb binaries using the minima hopping method [24,25] and calculated the theoretical convex hull of Bi-Sb. We not only discovered several energetically and thermodynamically stable crystal structures of Bi-Sb binaries

*smsingh@mix.wvu.edu

that are located on the convex hull, but we also recovered the known structures of Bi-Sb binaries in our structural search calculations. In the present work, we investigate the elastic and thermodynamic response of the stable Bi-Sb binaries. All the studied structures could be synthesized in laboratory under suitable ambient conditions [5,12,21–23].

Changes in the mechanical properties of Bi_xSb_{1-x} single crystals as a function of Sb concentration have been studied by ultrasonic wave velocity measurements at room temperature as well as at low temperatures [26–31]. In general, the elastic properties, i.e., bulk modulus, Young's modulus, and shear modulus, increase with increasing Sb concentration in Bi-Sb binaries [26]. Also, the average speed of sound increases with increasing Sb concentration; however, it decreases with increasing temperature [31]. Although most of the experiments report monotonous increase in the elastic moduli with increasing Sb concentration for larger atomic % of Sb, there exist some anomalies in the variation of the mechanical properties at low Sb concentration, which is consistent with our theoretical findings [26]. Although the specific heat of pristine Bi [32–35] and pristine Sb [36,37] has been studied in detail [35,37], little attention has been paid to the thermodynamic properties of Bi-Sb binaries [17,27,38]. Lichnowski and Saunders reported an increase in Debye temperature with increasing Sb concentration [27]. The effect of SOC on the elastic and mechanical properties of Bi-Sb binaries has not yet been reported in the literature, even though SOC is known to significantly change the electronic, vibrational, and thermodynamic properties of Bi- and Sb-based compounds [35,37,39].

In the present work, we report a systematic investigation of the elastic and thermodynamic properties of the Bi-Sb binaries calculated using first principles. We study the properties of the following Bi-Sb binary compositions (crystal structures are shown in Fig. 1): Bi_1Sb_7, Bi_1Sb_1, Bi_3Sb_1, Bi_7Sb_1, and Bi_9Sb_1, which lie on the convex hull of the Bi-Sb binary phase diagram (the only exception is the Bi_3Sb_1 composition which lies above, yet very close to, the convex hull) [12]. Our results indicate that the ductility of the structures increases with increasing Bi concentration, whereas, in general, the elastic moduli decrease with increasing Bi concentration. The bulk modulus (B), shear modulus (G), Young's modulus (E), Poisson's ratio (ν), and the elastic stiffness coefficients (C_{ij}) of the studied systems are reported below. We notice that Bi_1Sb_7, Bi_7Sb_1, and Bi_9Sb_1 monoclinic structures exhibit negative Poisson's ratio along different spatial directions. The Debye temperature and maximum heat capacity are found to increase with decreasing Bi concentration. Comparison of our theoretical findings with the available experimental data shows excellent agreement between theory and experiments.

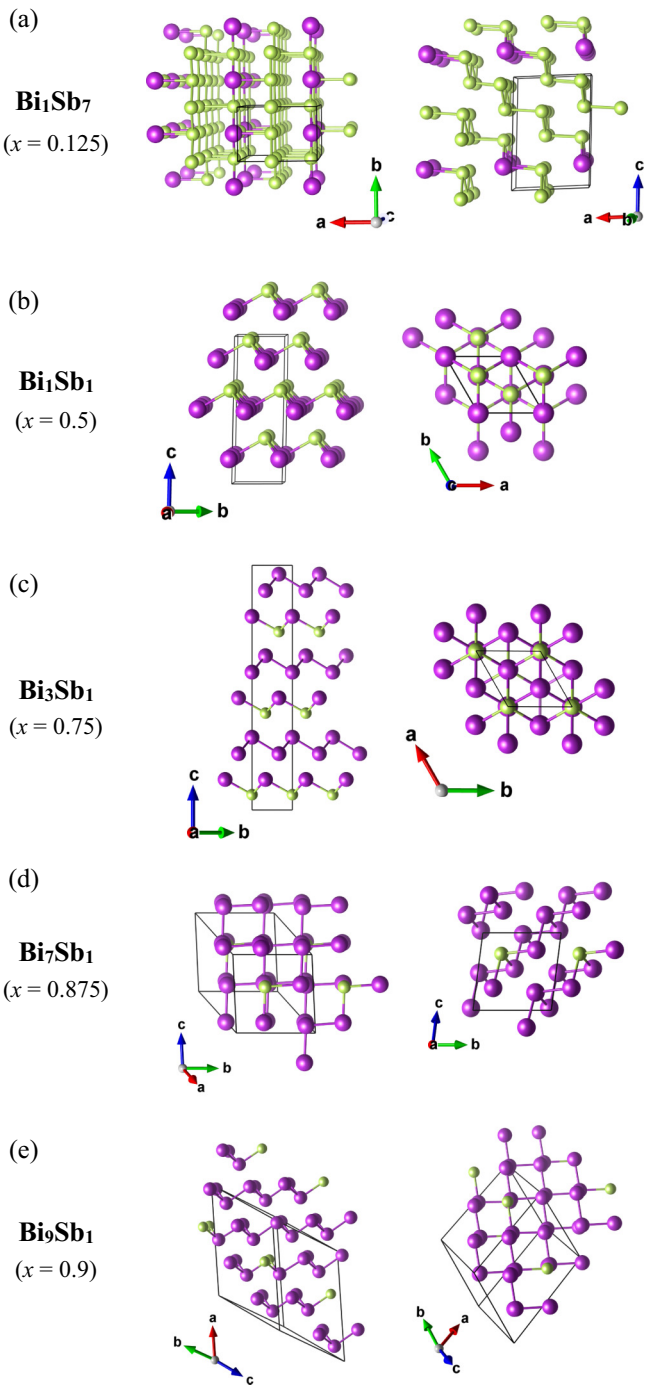

FIG. 1. The crystal structure of Bi-Sb binaries located on the Bi-Sb phase diagram [12]. Bi atoms are shown in purple, while Sb atoms are shown in green. Each crystal structure is shown from two different lattice orientations. The cutoff length for bonds was defined as 3.10 Å in Sb-rich compositions and 3.20 Å in Bi-rich compositions.

II. COMPUTATIONAL DETAILS

Density functional theory (DFT)-based first-principles calculations were carried out using the projector augmented-wave (PAW) method as implemented in the VASP code [40,41]. We used the PBE exchange-correlation functional as parametrized by Perdew, Burke, and Ernzerhof [42]. We considered 15 valence electrons of Bi ($5d^{10}6s^26p^3$) and five valence electrons of Sb ($5s^25p^3$) in the PAW pseudopotential. The lattice parameters of each structure were optimized until the Hellmann-Feynman residual forces were less than 10^{-4} eV/Å per atom. For convergence of the electronic self-consistent calculations, a total-energy difference criterion was defined as 10^{-8} eV. We used 650 eV as the kinetic-energy cutoff of the plane-wave basis set. We employed a Γ-type k mesh for hexagonal and trigonal structures, while a Monkhorst-pack-type k mesh was

TABLE I. List of elastic constants (C_{ij}) calculated with SOC (PBE+SOC) and without SOC (PBE). C_{ij} values (in GPa units) calculated with PBE+SOC are given in parentheses. x represents the concentration of Bi in Bi_xSb_{1-x}. The space group of each composition is given in the square brackets.

Composition	x	C_{11}	C_{22}	C_{33}	C_{44}	C_{55}	C_{66}	C_{12}	C_{13}	C_{23}	C_{15}	C_{25}	C_{35}	C_{46}
Sb [166]	0.0	92.2		35.8	29.8			21.8	20.3					
		(89.3)		(38.9)	(28.3)			(22.5)	(20.4)					
Theory [a]		91		38	27			24	21					
Bi_1Sb_7 [06]	0.125	98.5	83.1	36.2	36.8	13.0	16.2	6.4	12.7	32.0	15.1	6.4	1.9	6.8
		(95.1)	(81.5)	(37.4)	(34.0)	(13.7)	(15.2)	(7.2)	(13.0)	(30.9)	(13.2)	(5.4)	(2.3)	(6.5)
Bi_1Sb_1 [160]	0.5	75.5		29.1	13.4			21.8	18.0					
		(68.7)		(31.2)	(12.4)			(22.6)	(19.6)					
Bi_3Sb_1 [160]	0.75	67.3		31.0	7.8			27.0	20.7					
		(58.0)		(34.0)	(8.3)			(25.4)	(21.8)					
Bi_7Sb_1 [08]	0.875	61.6	63.4	26.3	4.2	5.8	20.7	23.1	16.9	17.8	1.6	−4.1	−0.6	−4.3
		(54.6)	(58.1)	(29.5)	(3.9)	(4.5)	(18.3)	(23.2)	(18.7)	(18.6)	(0.63)	(−3.3)	(0.6)	(−4.2)
Bi_9Sb_1 [08]	0.9	25.7	64.5	62.4	20.5	8.1	6.6	16.5	16.8	20.9	−0.5	−5.5	5.7	−4.5
		(30.0)	(66.3)	(55.2)	(15.8)	(10.7)	(0.5)	(16.7)	(15.4)	(18.8)	(−4.4)	(−5.6)	(2.9)	(−0.9)
Bi [166]	1.0	68.6		31.7	6.0			27.8	21.3					
		(62.6)		(36.1)	(8.8)			(25.6)	(23.3)					
Theory[a]		68		30	10			24	19					
Theory[b]		67.7		40.6	8.7			25.0	24.3					
Expt.[c]		69.3		40.4	13.5			24.5	25.4					
Expt.[d]		68.7		40.6	12.9			23.7						

[a]Reference [50] data from materials project database.
[b]Reference [51] data from LDA+SOC calculations.
[c]Reference [27] experiment was performed at 4.2 K. For high-temperature C_{ij} values for Bi, see Ref. [27] and references therein.
[d]Reference [52] experiment was performed at 4.2 K.

used to sample the irreducible Brillouin zone of all other crystal phases. The size of the k mesh was large enough to ensure the numerical convergence of total energy to less than 1 meV/atom.

The elastic constants C_{ij} were calculated using the stress-strain relationship as implemented in the VASP code. Elastic constants were converged better than 1 GPa by increasing the k-mesh size. The bulk modulus (B), shear modulus (G), Young's modulus (E), and Poisson's ratio (ν) quantities were first determined using the Voigt bound [43] and Reuss bound [44] schemes, and then an arithmetic average was computed following the Voigt-Reuss-Hill averaging scheme [45]. This way of evaluating elastic moduli is important since the Voigt and Reuss bounds give an upper and lower estimate of the actual elastic moduli of polycrystalline crystals, respectively. The Voigt bound scheme [43] relies on the assumption of uniform strain throughout the crystal, whereas the Reuss bound scheme [44] relies on the assumption of uniform stress throughout the crystal. Since SOC plays an important role in describing the electronic and vibrational properties of Bi and Sb atoms [35,37,39], we decide to investigate the effect of SOC on the elastic and mechanical properties of Bi-Sb binaries. Therefore, we have calculated elastic constants and elastic moduli for each studied structure twice: once with SOC and once without SOC. The PHONOPY code [46,47] was used to calculate the heat capacity of the crystal lattice.

In order to facilitate the analysis of elastic and mechanical properties, we have developed an open-source PYTHON code named MECHELASTIC [48], which can be used to evaluate many important physical quantities such as elastic moduli, elastic wave velocities, Debye temperature, melting temperature, and anisotropy factors, and perform the mechanical stability test for any crystalline bulk material. In the future, this code will be generalized for 3D as well as 2D systems.

III. RESULTS AND DISCUSSIONS

A. Elastic constants

The crystal structures of all the binary compounds under investigation are shown in Fig. 1. It is important to first discuss the elastic stiffness constants and define their relationship with the macroscopically measurable quantities that give us information about the elastic and mechanical properties of the system. The bulk modulus (B), Young's modulus (E), shear modulus (G), and Poisson's ratio (ν) are known as the elastic moduli and are macroscopically measurable quantities that give a measure of the elasticity of the material. These quantities can be determined from the elastic constants, C_{ijkl}. These constants are obtained through the use of the generalized stress-strain Hooke's law [49],

$$\sigma_{ij} = C_{ijkl}\epsilon_{kl}, \tag{1}$$

where σ_{ij} and ϵ_{kl} are the tensile stress and longitudinal strain, respectively. Utilizing the crystal symmetry operations, the total number of constants can be reduced from 81 to 3, 5, 6, and 13 for cubic, hexagonal, tetragonal, and monoclinic structures, respectively [49]. Table I lists the values of the relevant elastic constants calculated with and without inclusion of SOC. Although few nondiagonal elements of the C_{ij} matrix contain negative values for Bi_7Sb_1 and Bi_9Sb_1 binaries, all six eigenvalues of the C_{ij} matrix are positive, suggesting the

elastic stability of these binaries. In fact, all the eigenvalues of the C_{ij} matrix are positive for each studied Bi-Sb binary.

We notice a small yet significant change in the C_{ij} values due to the SOC effects. Notably, SOC is known to considerably change the electronic and vibrational spectra of Bi- and Sb-based compounds. Ramifications of SOC on the electronic band structure chiefly depend upon the crystal symmetry and, therefore, SOC could have different implications on the same composition but with different crystal symmetry [12,39]. Moreover, Díaz-Sánchez *et al.* [39] have reported that the dynamical properties and the interatomic force constants of Bi are very sensitive to the strength of the SOC. They reveal that SOC softens the phonon modes in Bi by about 10% and yields remarkable agreement when compared to that of the experimental values. However, SOC has much smaller effects on the lattice parameters [39]. In a similar work, Serrano *et al.* [37] have studied the effects of SOC on the specific heat, the lattice parameter, and the cohesive energy of Sb. Their calculations reveal that all these quantities depend almost quadratically on the SOC strength. [37] The small change in the C_{ij} values due to SOC can be attributed to the above-mentioned reasons. The calculated elastic constant values are consistent with an experimental work reported by Lichnowski *et al.* [27], where they investigated the elastic properties of $Bi_{1-x}Sb_x$ ($0.03 < x < 0.1$) single crystals for small Sb concentration.

Notably, the strength of SOC in Sb is much smaller compared to that in Bi; consequently, changes in the C_{ij} values for Sb-rich compositions are relatively less (slightly over our convergence criteria of 1.0 GPa) compared to that in the Bi-rich compositions. However, we do notice considerable SOC-induced changes in the C_{ij} values for Bi-rich compositions. The influence of SOC on the C_{ij} (to increase or decrease the C_{ij} and therefore the stiffness) is fairly uniform across all compositions. Even pure Sb and Bi follow the same trends, with the exception of C_{12}. These trends indicate that in general, due to the SOC effects, Bi_xSb_{1-x} becomes less stiff along the x and y major axes for deformations along the x and y directions, more stiff along the z major axis for deformation along the z direction, and differ for the transverse forces and responses in the x-y plane. In general, SOC effects cause elastic softening in all directions perpendicular to the z axis. The observed elastic softening could be associated to the SOC-induced softening of phonon modes [39]. In a previous work, Arnaud *et al.* [51] investigated the effect of SOC on the elastic properties of Bi and observed a similar SOC-induced elastic softening. Their reported values are in good agreement with our data presented in Table I. Here, we would like to note the peculiar effect of SOC on the Bi-rich compound, Bi_9Sb_1. In Bi_9Sb_1, we see that the aforementioned trends are reversed for most of the C_{ij} values. Also, anomalous changes in the elastic stiffness constants can be observed for Bi_9Sb_1, which will be discussed in more detail later. These changes support the before-mentioned complex relationship between the SOC and the electronic and phonon band structure, leading to directional changes in the bonding within the material.

Our calculations indicate that SOC causes small changes (overall less than 1.0 %) in the Bi-Sb, Bi-Bi, and Sb-Sb bond lengths, which when combined with the phonon softening could be held accountable for the observed SOC-induced changes in the C_{ij} values. The maximum variation in the bond length due to SOC is within the range of ± 0.03 Å. Further details of the bond lengths, lattice parameters, electronic band structure, and phonon band structure of all studied structures can be found in Ref. [12]. Since elastic constants are defined in terms of free energy with respect to strain, the following conclusion can be made here: in the presence of SOC, electrons in material are redistributed to minimize the total free energy, thereby recovering some of the strain energy and reducing the effective elastic stiffness.

B. Mechanical properties

We further test the mechanical stability of all the studied structures. A material can be considered mechanically stable if it passes the Born-Huang mechanical stability criteria [49,53]. This criteria states that in order to be mechanically stable, the Gibbs free energy of any relaxed crystal, i.e., in the absence of any external load, must be minimum compared to any other state reached by means of an infinitesimal strain. This requires that the elastic stiffness matrix C_{ij} is positive definite, i.e., all the eigenvalues of C_{ij} are positive and the matrix is symmetric. Additionally, all the leading principle minors and any arbitrary set of minors (trailing minors) of C_{ij} must be positive. If a crystal, regardless of its symmetry, satisfies the aforementioned conditions, it can be considered mechanically stable. The mathematical expressions for these conditions have been reported for different crystal classes by various research groups [54–57]. It is important to mention here that in some of the published papers [54–56], these conditions are incorrectly generalized from the cubic criteria (especially for the lower-symmetry structures), which could lead to a wrong quantitative analysis. However, it could not change the qualitative picture of mechanical stability of a crystal. Mouhat and Coudert correctly generalized the Born-Huang mechanical stability conditions for all crystal classes [57]. Therefore, we refer the reader to the seminal paper of Mouhat and Coudert for further details regarding the necessary and sufficient conditions for the mechanical stability conditions [57]. In our case, we find that all the studied Bi-Sb binary structures pass the Born-Huang mechanical stability test and hence can be considered mechanically stable.

Once the C_{ijkl} constants are calculated, the four moduli (B, G, E, and ν) can be obtained by using relations between the constants [58]. Details of these relations for different crystal systems, and for Voigt and Reuss bound schemes, are summarized in Ref. [56]. The bulk modulus represents the volume compressibility of the material and is given by $B = E/3(1 - 2\nu)$ [49]. Young's modulus gives a measure of the stiffness of the system. It is simply the ratio of the stress along an axis to strain along that axis. A material is very stiff if it has large E. Poisson's ratio is used as a measure of plasticity as it measures the expansion of material in the transverse direction to the direction of compression. It is calculated using $\nu = (3B - 2G)/2(3B + G)$. The shear modulus, or the modulus of rigidity, describes the deformation of the system under transverse internal forces. It is related to Young's modulus and the Poisson ratio by $G = E/2(1 + \nu)$. A way to measure the brittleness or ductility of a material comes from the ratio of the bulk modulus to the shear modulus, B/G ratio, with values above 1.7 giving ductile behavior [58,59].

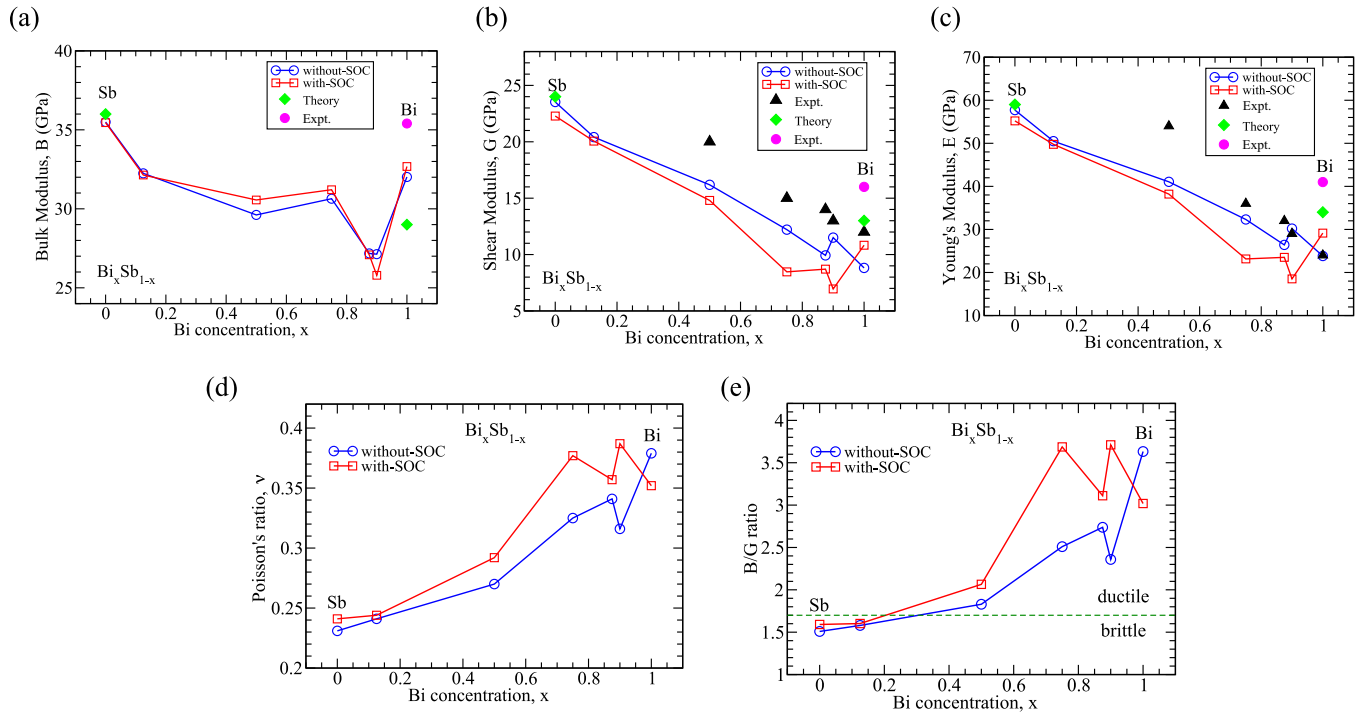

FIG. 2. Mechanical properties of Bi-Sb binaries calculated with and without inclusion of SOC: (a) bulk modulus B (in GPa), (b) shear modulus G (in GPA), (c) Young's modulus E (in GPA), (d) Poisson's ratio ν, and (e) B/G ratio. The green dotted line in (e) shows the boundary ($B/G = 1.7$) below (above) which the material behaves as brittle (ductile). Experimental data at room temperature (black triangles) is from Ref. [26], theoretical data (green diamonds) is from Ref. [50], and experimental data at 4.2 K (purple circles) is from Ref. [27].

Figures 2(a)–2(c) show the observed variation in the B,G, and E values as a function of Bi concentration in Bi_xSb_{1-x}. Red (blue) represents the data points calculated with (without) inclusion of SOC. We notice that B,G, and E values systematically decrease with increasing Bi concentration, but the change in B is relatively less compared to that for G and E. As expected, the effects of SOC are more dominant towards the Bi-rich side than that towards the Sb-rich side. We notice that in all moduli except B, these effects on the Bi-rich compositions are present, and the same reversal in trends mentioned in the previous section can be seen in Bi_9Sb_1.

The available experimental and theoretical data (given in Fig. 2) are in excellent agreement with our theoretical calculations [26,27,50]. Here, it important to mention that all the theoretical values are lower than that of the experimental observations. This is due to the fact that we used the generalized gradient approximation (GGA) in all of our calculations, and GGA is well known to underestimate the elastic constant values [56]. We also notice that the Poisson's ratio (ν) and B/G ratio increase with increasing Bi concentration, indicating an increase in the ductile behavior of Bi-rich compositions. This could be associated to a decrease in the strength of the covalent bonds in Bi-rich compositions. The Bi-Bi bond length in pristine Bi (3.10 Å) is considerably larger compared to the Sb-Sb bond length in pristine Sb (2.96 Å), thus suggesting stronger covalent bonding in Sb. The average bond length increases with increase in the Bi concentration. The bond lengths are as follows: in pristine Sb, the Sb-Sb bond = 2.96 Å; in Bi_1Sb_7, the Sb-Sb bond = 2.98 Å; in Bi_1Sb_1, the Bi-Sb bond = 3.04 Å; in Bi_3Sb_1, the Bi-Sb bond = 3.03 Å and the Bi-Bi bond = 3.09 Å; in Bi_7Sb_1, the Bi-Sb bond = 3.02 Å and the Bi-Bi bond = 3.10–3.12 Å; in Bi_9Sb_1, the Bi-Sb bond = 3.05 Å and Bi-Bi = 3.12 Å; and in pristine Bi, the Bi-Bi bond = 3.10 Å. Consequently, the increasing bond length causes a decrease in the elastic moduli and increase in the ν and B/G values. The observed variation in the mechanical properties is consistent with changes in the bond length. Thus, a monotonic decrease in B,G, and E values with increasing Bi concentration can be correlated with decreasing valence electron density [60]. However, the anomalies observed in the elastic properties of the Bi_9Sb_1 composition with low Sb concentration that are consistent with previous experimental studies [26] warrant a further investigation of this issue. The first-principles calculations using virtual crystal approximation (VCA), which are beyond the scope of the present work, can offer good insights to resolve this issue. The possible reasons behind the observed anomalies in the properties of Bi_9Sb_1 are discussed below.

C. Negative Poisson's ratio

Materials having negative Poisson's ratio (ν), known as auxetic materials, have attracted the special attention of researchers due to their exceptional advantages in sensing technology [62–68]. As we mentioned earlier, a positive Poisson's ratio defines the ratio of the transverse contraction to the longitudinal extension of a material during the stretching process. Therefore, materials with negative Poisson's ratio, i.e., auxetic materials, are expected to expand in the transverse direction when stretched in the longitudinal direction. Auxetic

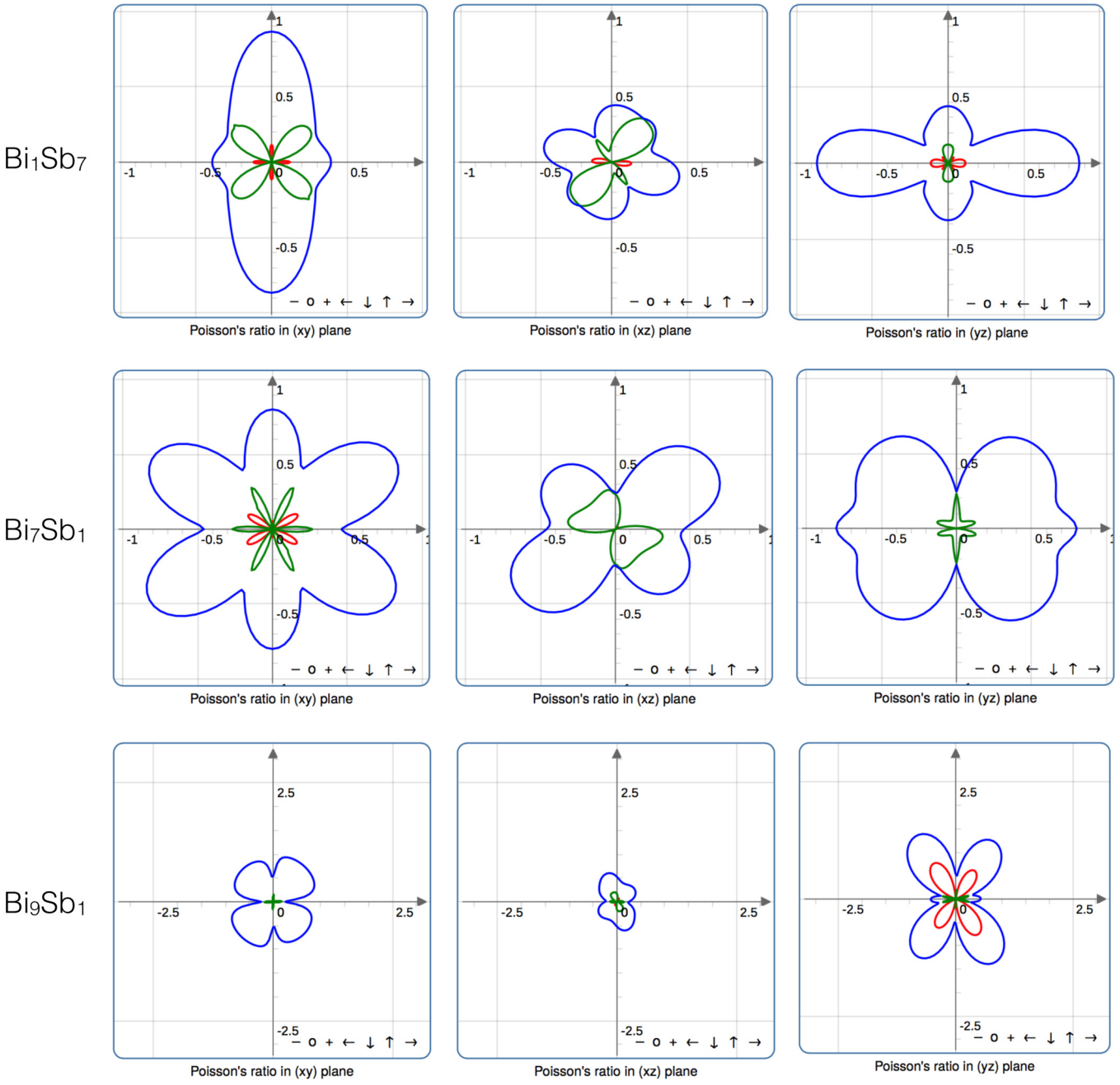

FIG. 3. Top, middle, and bottom panels represent the calculated Poisson's ratio of Bi_1Sb_7, Bi_7Sb_1, and Bi_9Sb_1 binaries, respectively. All plots were generated using the ELATE software [61]. Green (red) corresponds to the positive (negative) values of ν (see text for details).

materials are quite rare in nature as compared to nonauxetic materials. However, Baughman *et al.* [64] reported that the auxetic property is often observed in cubic elemental metals. Interestingly, auxetic materials with lower symmetry are more appealing for technological applications because they yield much larger strain amplification as compared to the highly symmetric auxetic materials [65]. In order to analyze the auxeticity of the studied structures, we thoroughly investigate the elastic tensor of each studied composition calculated with SOC.

Using the open-source ELATE software tool [61,69], we have analyzed the spatial variation of Poisson's ratio for each studied structure. We observe that three out of seven binary structures exhibit significantly large negative Poisson's ratio along different spatial directions. All these structure belong to the low-symmetry (monoclinic) space groups; therefore, these structures are more advantageous for technological applications. The results are given in Fig. 3. Regarding the theoretical details of these plots, we refer the reader to the excellent paper of Gaillac *et al.* [69]. In spherical coordinates, the determination of ν requires an extra dimension in addition to the $\theta(0,\pi)$ and $\phi(0,2\pi)$ coordinates, i.e., $\nu(\theta,\phi,\chi)$. The additional dimension can be characterized by an angle $\chi(0,2\pi)$ [69,70]. The blue color in Fig. 3 represents the surface obtained at the maximum of χ, whereas the green (red) lobes correspond to the positive (negative) values of ν obtained at the minimum

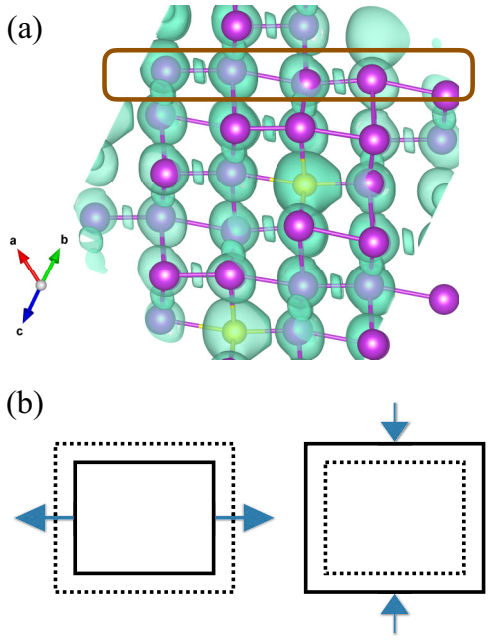

FIG. 4. (a) Distribution of electron localization function (turquoise) in monoclinic Bi_9Sb_1 plotted at isosurface value $\eta = 0.25$. Purple: Bi atoms; yellow: Sb atoms. The hinge structure or bowtie structure of the Bi-Bi bonds can be noticed in the selected region. (b) Illustration of the negative Poisson's effect under compression (left) and expansion (right) on auxetic materials. The dotted square represents the deformed shape of the original structure (solid lines) and the arrows represent the direction of strain.

of χ. We find that the Bi_9Sb_1 monoclinic structure exhibits the largest negative Poisson's ratio in the y-z plane. The minimum value of ν is ~ -0.6, which is comparable with the value $\nu_{\min} = -0.8$ reported for polymer foam structures by Lakes *et al.* [63]. The other two monoclinic structures, Bi_1Sb_7 and Bi_7Sb_1, inherit relatively smaller negative Poisson's ratio.

In order to understand the microscopic origin of negative Poisson's ratio, we analyze the geometry of the bonds and the distribution of electron localization function along the bond directions in Bi_9Sb_1, as shown in Fig. 4(a). One can notice that the atomic bonds in Bi_9Sb_1 form a hinge- or bowtielike structure in the y-z plane. Such structural arrangement has been reported to yield negative Poisson's ratio in auxetic materials (see Fig. 1 of Ref. [67]). A linear chain of Bi-Bi atoms forming inverted hexagon or hingelike bonds can be noticed in the highlighted region of Fig. 4(a). Plotting the electron localization function reveals that two adjacent Bi-Bi bonds inherit opposite features in their electron distribution. Along one bond there exists overlap of charges in the middle, indicating the bonding nature of orbitals from the two nearest Bi atoms, whereas along the consecutive Bi-Bi bond, no such charge overlap is present, indicating an antibonding feature or the presence of a charge nodal plane at the middle of the Bi-Bi bond. Such two adjacent bonds could form orthogonal hinges, which are responsible for the observed auxetic behavior in Bi_9Sb_1. A similar concept can be applied to explain the auxeticity of Bi_1Sb_7 and Bi_7Sb_1 monoclinic structures. Due to the intrinsic hinge structures, in the presence of compressive strain along the longitudinal direction, these structures tend to shrink in the transverse direction, and vice versa. Figure 4(b) illustrates the behavior of an auxetic material in the presence of compressive or tensile strain.

D. Elastic wave velocities, Debye temperature, and melting temperature

Knowledge of the elastic wave velocities, Debye temperature, and melting temperature is important for practical applications. Therefore, we estimate these quantities using the MECHELASTIC code [48]. We calculate the longitudinal (v_l), transverse (v_t), and average (v_m) elastic wave velocities using the following relations [71,72]:

$$v_l = \sqrt{\frac{3B + 4G}{3\rho}}, \tag{2}$$

$$v_t = \sqrt{\frac{G}{\rho}}, \tag{3}$$

$$\frac{1}{v_m} = \left[\frac{1}{3}\left(\frac{2}{v_t^3} + \frac{1}{v_l^3}\right)\right]^{-1/3}, \tag{4}$$

where B and G are the bulk and shear moduli, and ρ is the density of material. Conversely, one can also determine the elastic stiffness constants by measuring the distance traveled by an ultrasonic wave pulse and the corresponding time.

Debye temperature (Θ_D) is another important parameter that we can estimate from the knowledge of the elastic wave velocities and the density of material. Debye temperature correlates with several important physical properties such as specific heat, elastic constants, ultrasonic wave velocities, and melting temperature. At low temperatures, acoustic phonons are the only vibrational excitations that contribute to the specific heat. Therefore, at low temperatures, the Debye temperature calculated from the elastic constants is the same as the Θ_D obtained from the specific-heat measurements. We calculate Θ_D using the following equation [71]:

$$\Theta_D = \frac{h}{k_B}\left[\frac{3q}{4\pi}\frac{N\rho}{M}\right]^{1/3} v_m, \tag{5}$$

where h is the Planck's constant, k_B is the Boltzmann's constant, q is the total number of atoms in the cell, N is the Avogadro's number, ρ is the density, and M is the molecular weight of the solid. The melting temperature was estimated using the empirical relation $T_{\text{melt}} = 607 + 9.3B \pm 555$ [73].

Table II contains a list of the v_l, v_t, v_m, Θ_D, and T_{melt} values calculated with and without inclusion of SOC. We notice that the magnitude of the elastic wave velocities and Θ_D decreases due to the SOC effects, which can be associated to the SOC-induced elastic softening. Figure 5 shows variation in the elastic wave velocities and Θ_D as a function of the Bi concentration. In general, we observe a monotonic decrease in the mentioned quantities with increasing Bi concentration. However, anomalies from the monotonic trend can be noticed at low Sb concentration. This observation is consistent with the previous experimental studies of Gopinathan *et al.* [26] and Lichnowski *et al.* [27], where the authors investigated the elastic properties of Bi_xSb_{1-x} crystals using ultrasonic waves. The experimental Θ_D values for pristine Sb and pristine Bi at

TABLE II. List of the longitudinal (v_l), transverse (v_t), and average (v_m) elastic wave velocities, as well as the Debye (Θ_D) and melting (T_{melt}) temperatures, calculated with SOC (PBE+SOC) and without SOC (PBE). Values calculated with PBE+SOC are given in parentheses. The space group of each composition is given in square brackets.

Composition	v_l (m/s)	v_t (m/s)	v_m (m/s)	Θ_D (K)	T_{melt} (K)
Sb [166]	3240	1946	2152	202.4	930
	(3256)	(1945)	(2152)	(202.4)	(937)
Expt.[a]				209.6	
Expt.[b]				210.0	
Expt.[c]				211.3	
Expt.[d]				211.3	
Bi_1Sb_7 [06]	2941	1714	1902	177.2	904
	(2943)	(1712)	(1899)	(177.0)	(906)
Bi_1Sb_1 [160]	2548	1432	1593	145.0	881
	(2519)	(1372)	(1531)	(139.3)	(887)
Bi_3Sb_1 [160]	2308	1151	1291	116.5	893
	(2260)	(1077)	(1211)	(109.2)	(893)
Bi_7Sb_1 [08]	2123	1050	1179	105.0	856
	(2097)	(975)	(1098)	(98.0)	(863)
Bi_9Sb_1 [08]	2158	1131	1265	112.5	850
	(1989)	(885)	(999)	(88.9)	(847)
Bi [166]	2197	1071	1203	108.2	901
	(2237)	(1102)	(1237)	(111.3)	(908)
Expt.[e]				112	

[a]Reference [77],
[b]Reference [78],
[c]Reference [79] data from specific-heat measurements at low temperatures.
[d]Reference [80] data from thermal expansion measurements.
[e]Reference [81] data evaluated from the sound velocity measurements.

low temperature are ∼210 and ∼112 K, which are in excellent agreement with our theoretical findings.

Anomalous changes in the electronic, thermal, elastic, and mechanical properties of Bi_xSb_{1-x} at very low Sb concentration have often been noted in experiments. Bi_xSb_{1-x} undergoes a semimetal-semiconductor phase transition in the Sb-concentration range $0.07 < x < 0.22$, and a topological nontrivial insulator phase appears due to the inverted ordering of bands at the L point of the Brillouin zone [7,8,74,75]. Rogacheva *et al.* [76] studied the effect of low Sb concentration on the lattice parameters, microhardness, electrical conductivity, magnetoresistance, and the Seebeck coefficient of Bi_xSb_{1-x}.

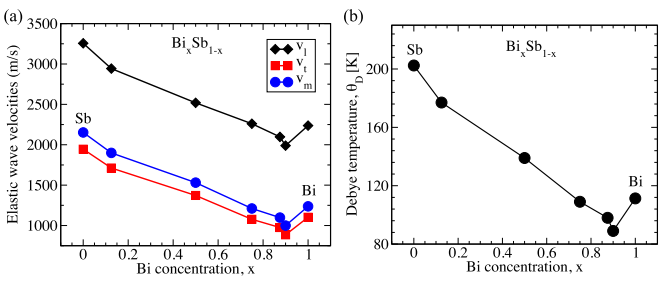

FIG. 5. (a) Elastic wave velocities and (b) Debye temperature (Θ_D) of Bi-Sb binaries calculated with SOC.

Their experiments revealed an anomalous change in the properties of Bi_xSb_{1-x} at small x values, which were attributed to the percolation transition, geometric reordering of atoms, and semimetal-semiconductor electronic phase transition. They further argued that at low Sb concentration, the elastic fields of neighboring atoms begin to overlap, causing partial compensation of elastic stress with reversed signs, which leads to an abrupt decrease in the elastic stiffness of the entire crystal [76]. For this reason, at low Sb concentration, Bi_xSb_{1-x} exhibits a rapid decrease in the microhardness, electrical conductivity, and Seebeck coefficient. Increasing Sb concentration beyond a critical value yields the formation of new atomic ordering, causing enhancement in the elastic and mechanical properties of Bi_xSb_{1-x}. The same argument can be used to explain the observed variation in the elastic wave velocities and Debye temperature of Bi_xSb_{1-x} with varying x (see Fig. 5).

E. Specific heat

After evaluating the elastic properties and mechanical stabilities of the Bi-Sb binaries, we focus our attention on the specific heat (C) of the crystal lattice. Before we start our discussion, it is important to mention that at low temperatures (T), the difference between $C_p(T)$ (at constant pressure) and $C_v(T)$ (at constant volume) is almost negligible and it lies within the uncertainty range of the experiments [82]. Therefore, we do not make any distinction between $C_p(T)$ and $C_v(T)$ in the present work. In the low-T limit, the general relationship between $C(T)$ and T can be described using the following expression:

$$C(T) = \gamma T + \beta T^3 + \alpha T^{-2}, \tag{6}$$

where the first and second terms correspond to the electronic and crystal lattice contributions to the specific heat, whereas the last term addresses the interaction of the nuclear quadrupole moment with the electric-field gradient of electrons and lattice. The last term is very small even at low temperatures; however, it might become substantial below 1 K [37]. Usually at low T, the specific heat follows the T^3 power law due to the dominant contribution from the lattice vibrations. Therefore, plotting $C(T)/T^3$ versus T is a good way to determine the contribution of the lattice vibrations in the net heat capacity [37,82–84]. The peak appearing in this plot is the evidence of the deviation from the Debye behavior that is known to separate the contribution of the acoustic phonons and optical phonons in the total specific heat of the material. From the observed position of the peak in the $C(T)/T^3$ versus T plot, one can estimate the Einstein's oscillator temperature, which is typically equal to $\sim 6T_0$, where T_0 is the temperature corresponding to the maximum, $C(T)/T^3$ [82,84].

Figure 6 shows the $C(T)/T^3$ versus T plots for all the studied binaries. SOC was not included in the calculation of $C(T)$. The corresponding phonon dispersion for each structure is given in Ref. [12]. Noticeably, the peak height in the $C(T)/T^3$ versus T plot significantly increases (more than three times) with increasing Bi concentration from Bi_1Sb_7 to Bi_9Sb_1. Also, the peak shifts towards lower T with increasing Bi concentration, indicating a decrease in Θ_D as we go towards the Bi-rich side. This is consistent with Θ_D obtained from the elastic constants calculations, and it can be associated to the

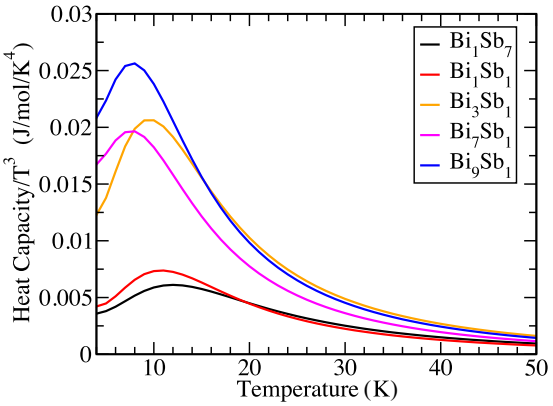

FIG. 6. $C(T)/T^3$ vs temperature T data for Bi-Sb binaries.

decrease in the average strength of the covalent bonds in Bi-rich binaries. We further compare our results with the available theoretical and experimental reports on the pristine Bi [32–35], pristine Sb [36,37], and Bi-Sb [27] binaries. Our findings are in remarkable agreement with the reported data in the literature. Lichnowski and Saunders [27] have experimentally observed a decrease in Θ_D with increasing Bi concentration. The accepted T_0 values for pristine Sb and pristine Bi are 7.5 and 14 K, respectively [35,37]. In agreement, we also notice an overall shift of the T_0 towards lower temperatures from 12 K (for Sb-rich composition) to 8 K (for Bi-rich composition).

Finally, we would like to remark on the effect of SOC on the specific heat of the studied binaries. Undoubtedly, SOC is expected to have significant effects on the thermodynamic properties of Bi-rich binaries. In particular, the SOC effects in Bi cause an enhancement in the $C(T)/T^3$ peak height and decrement in the Θ_D value by $\sim$1 K, thereby reducing the discrepancies between the experimental heat capacity data and *ab initio* results [35]. However, SOC is found to have negligible effects on the thermodynamic properties of pristine Sb [37]. This is the reason why our results (calculated without inclusion of SOC) for Sb-rich binaries compare well with the experimental observations, while there exists a small inconsistency in the data of Bi-rich compositions (for example, Bi_9Sb_1). Including SOC effects in the calculations would yield better agreement with the experimental data, specifically for Bi-rich compositions. Nevertheless, SOC-induced changes in the T_0 values are expected to be within $\pm$1 K range.

IV. CONCLUSION

In this work, we have investigated the elastic, mechanical, and thermodynamic properties of several energetically stable Bi-Sb binary structures. We find that bulk, shear, and Young's moduli increase with increasing Sb concentration in Bi_xSb_{1-x}, and decrease as we move towards the Bi-rich side. However, Poisson's ratio and B/G ratio increase with increasing Bi concentration, suggesting more ductile behavior in Bi-rich compositions. Our calculations reveal that Bi_1Sb_7, Bi_7Sb_1, and Bi_9Sb_1 monoclinic structures exhibit negative Poisson's ratio, indicating auxeticity along different spatial directions. The hinge structure of atomic bonds is the main source of negative Poisson's ratio in these structures. We also probe the effect of SOC on the elastic and mechanical properties of Bi-Sb binaries. In general, the SOC effects cause elastic softening in most of the studied structures, which can be ascribed to the fact that in the presence of SOC, electrons are redistributed to minimize the total free energy, thereby recovering some of the strain energy and reducing the effective elastic stiffness. Our calculations reveal that the Debye temperature and the magnitude of the elastic wave velocities monotonically decrease with increasing Bi concentration. This can be ascribed to the decreasing strength of covalent bonds (i.e., larger bond length) in the Bi-rich compositions. However, we observe some anomalies in the elastic properties of Bi-rich composition Bi_9Sb_1, which requires further investigation. The peak of $C(T)/T^3$ shifts towards lower temperatures and increases in height with increasing Bi concentration. We find that SOC plays an important role in the determination of the properties for Bi-rich compositions, while the effects of SOC are very small for Sb-rich compositions. Our overall results are consistent with the available experimental data.

ACKNOWLEDGMENTS

This work used the Extreme Science and Engineering Discovery Environment (XSEDE), which is supported by National Science Foundation Grant No. OCI-1053575. Additionally, the authors acknowledge the support from the Texas Advances Computer Center (TACC), Bridges supercomputer at Pittsburgh Supercomputer Center, and Super Computing Systems (Spruce and Mountaineer) at West Virginia University (WVU). A.H.R. and S.S. acknowledge the support from National Science Foundation (NSF) DMREF-NSF Project No. 1434897 and the U.S. Department of Energy Project No. DE-SC0016176. S.S. also acknowledges the financial support from the Jefimenko Fellowship, Robert T. Bruhn Research Award, and the WVU Foundation Distinguished Doctoral Scholarship at WVU. We thank the anonymous referee for providing us with important insights which helped us to facilitate the reported analysis of the negative Poisson's ratio.

[1] A. Ibrahim and D. Thompson, Mater. Chem. Phys. **12**, 29 (1985).
[2] B. Lenoir, A. Dauscher, X. Devaux, R. Martin-Lopez, Yu. I. Ravich, H. Scherrer, and S. Scherrer, in *Proceedings of the 15th International Conference on Thermoelectrics* (IEEE, New York, 1996), pp. 1–13.
[3] W. Yim and A. Amith, Solid-State Electron. **15**, 1141 (1972).
[4] B. Lenoir, M. Cassart, J.-P. Michenaud, H. Scherrer, and S. Scherrer, J. Phys. Chem. Solids **57**, 89 (1996).
[5] H. Y. Lv, H. J. Liu, L. Pan, Y. W. Wen, X. J. Tan, J. Shi, and X. F. Tang, J. Phys. Chem. C **114**, 21234 (2010).
[6] L. Fu and C. L. Kane, Phys. Rev. B **76**, 045302 (2007).
[7] D. Hsieh, D. Qian, L. Wray, Y. Xia, Y. S. Hor, R. J. Cava, and M. Z. Hasan, Nature (London) **452**, 970 (2008).

[8] J. C. Y. Teo, L. Fu, and C. L. Kane, Phys. Rev. B **78**, 045426 (2008).
[9] H.-J. Zhang, C.-X. Liu, X.-L. Qi, X.-Y. Deng, X. Dai, S.-C. Zhang, and Z. Fang, Phys. Rev. B **80**, 085307 (2009).
[10] M. Z. Hasan and C. L. Kane, Rev. Mod. Phys. **82**, 3045 (2010).
[11] S. Singh, A. C. Garcia-Castro, I. Valencia-Jaime, F. Muñoz, and A. H. Romero, Phys. Rev. B **94**, 161116 (2016).
[12] S. Singh, W. Ibarra-Hernández, I. Valencia-Jaime, G. Avendaño-Franco, and A. H. Romero, Phys. Chem. Chem. Phys. **18**, 29771 (2016).
[13] C. G. Tan, P. Zhou, J. G. Lin, and L. Z. Sun, Phys. Status Solidi (RRL) **11**, 1700051 (2017).
[14] W. Yu, C.-Y. Niu, Z. Zhu, X. Cai, L. Zhang, S. Bai, R. Zhao, and Y. Jia, RSC Adv. **7**, 27816 (2017).
[15] M. Brzezińska, M. Bieniek, T. Woźniak, P. Potasz, and A. Wójs, arXiv:1709.03935.
[16] S. Singh and A. H. Romero, Phys. Rev. B **95**, 165444 (2017).
[17] S. Lee, K. Esfarjani, J. Mendoza, M. S. Dresselhaus, and G. Chen, Phys. Rev. B **89**, 085206 (2014).
[18] G. Gutiérrez, E. Menéndez-Proupin, and A. K. Singh, J. Appl. Phys. **99**, 103504 (2006).
[19] J. Dismukes, R. Paff, R. Smith, and R. Ulmer, J. Chem. Eng. Data **13**, 317 (1968).
[20] H. Berger, B. Christ, and J. Troschke, Cryst. Res. Technol. **17**, 1233 (1982).
[21] A. Datta and G. S. Nolas, CrystEngComm **13**, 2753 (2011).
[22] H. Zhang, J. S. Son, J. Jang, J.-S. Lee, W.-L. Ong, J. A. Malen, and D. V. Talapin, ACS Nano **7**, 10296 (2013).
[23] K. Kaspar, K. Fritsch, K. Habicht, B. Willenberg, and H. Hillebrecht, J. Electron. Mater. **46**, 92 (2017).
[24] S. Goedecker, J. Chem. Phys. **120**, 9911 (2004).
[25] M. Amsler and S. Goedecker, J. Chem. Phys. **133**, 224104 (2010).
[26] K. K. Gopinathan and A. R. K. L. Padmini, J. Phys. D **7**, 32 (1974).
[27] A. J. Lichnowski and G. A. Saunders, J. Phys. C **9**, 927 (1976).
[28] M. Cankurtaran, H. Celik, and T. Alper, J. Phys. F **15**, 391 (1985).
[29] J. Dominec, J. Phys. C **18**, 5793 (1985).
[30] M. Cankurtaran, H. Celik, and T. Alper, J. Phys. F **16**, 853 (1986).
[31] M. Emuna, Y. Greenberg, E. Yahel, and G. Makov, J. Non-Cryst. Solids **362**, 1 (2013).
[32] P. H. Keesom and N. Pearlman, Phys. Rev. **96**, 897 (1954).
[33] T. C. Cetas, J. C. Holste, and C. A. Swenson, Phys. Rev. **182**, 679 (1969).
[34] D. G. Archer, J. Chem. Eng. Data **40**, 1015 (1995).
[35] L. E. Díaz-Sánchez, A. H. Romero, M. Cardona, R. K. Kremer, and X. Gonze, Phys. Rev. Lett. **99**, 165504 (2007).
[36] W. DeSorbo, Acta Metallurg. **1**, 503 (1953).
[37] J. Serrano, R. K. Kremer, M. Cardona, G. Siegle, L. E. Díaz-Sánchez, and A. H. Romero, Phys. Rev. B **77**, 054303 (2008).
[38] G. V. Bunton and S. Weintroub, J. Phys. C **2**, 116 (1969).
[39] L. E. Díaz-Sánchez, A. H. Romero, and X. Gonze, Phys. Rev. B **76**, 104302 (2007).
[40] G. Kresse and J. Furthmüller, Phys. Rev. B **54**, 11169 (1996).
[41] G. Kresse and D. Joubert, Phys. Rev. B **59**, 1758 (1999).
[42] J. P. Perdew, K. Burke, and M. Ernzerhof, Phys. Rev. Lett. **77**, 3865 (1996).
[43] W. Voigt, *Lehrburch Der Kristallphys* (Teubner Press, Leipzig, Germany, 1928).
[44] A. Reuss, Z. Angew. Math. Mech. **9**, 49 (1929).
[45] R. Hill, Proc. Phys. Soc. London, Sect. A **65**, 349 (1952).
[46] A. Togo, F. Oba, and I. Tanaka, Phys. Rev. B **78**, 134106 (2008).
[47] A. Togo and I. Tanaka, Scr. Mater. **108**, 1 (2015).
[48] S. Singh and A. H. Romero, computer code MECHELASTIC (unpublished), https://github.com/sobhitsinghphy/MechElastic.
[49] J. F. Nye, in *Physical Properties of Crystals* (Clarendon, Oxford, 1985), pp. 145 and 147.
[50] M. de Jong, W. Chen, T. Angsten, A. Jain, R. Notestine, A. Gamst, M. Sluiter, C. Krishna Ande, S. van der Zwaag, J. J. Plata, C. Toher, S. Curtarolo, G. Ceder, K. A. Persson, and M. Asta, Sci. Data **2**, 150009 (2015).
[51] B. Arnaud, S. Lebègue, and G. Raffy, Phys. Rev. B **93**, 094106 (2016).
[52] Y. Eckstein, A. W. Lawson, and D. H. Reneker, J. Appl. Phys. **31**, 1534 (1960).
[53] M. Born, K. Huang, and M. Lax, Am. J. Phys. **23**, 474 (1955).
[54] S. K. R. Patil, S. V. Khare, B. R. Tuttle, J. K. Bording, and S. Kodambaka, Phys. Rev. B **73**, 104118 (2006).
[55] Z. Wu, X. Hao, X. Liu, and J. Meng, Phys. Rev. B **75**, 054115 (2007).
[56] Z.-J. Wu, E.-J. Zhao, H.-P. Xiang, X.-F. Hao, X.-J. Liu, and J. Meng, Phys. Rev. B **76**, 054115 (2007).
[57] F. Mouhat and F.-X. Coudert, Phys. Rev. B **90**, 224104 (2014).
[58] S. Pugh, Philos. Mag. Ser. 7 **45**, 823 (1954).
[59] O. Pavlic, W. Ibarra-Hernandez, I. Valencia-Jaime, S. Singh, G. Avendaño-Franco, D. Raabe, and A. H. Romero, J. Alloys Compd. **691**, 15 (2017).
[60] M. C. Gao, Y. Suzuki, H. Schweiger, Ö. N. Doğan, J. Hawk, and M. Widom, J. Phys.: Condens. Matter **25**, 075402 (2013).
[61] R. Gaillac and F.-X. Coudert, computer code ELATE (unpublished), https://github.com/fxcoudert/elate.
[62] E. Kittinger, J. Tichý, and E. Bertagnolli, Phys. Rev. Lett. **47**, 712 (1981).
[63] R. Lakes, Science **235**, 1038 (1987).
[64] R. H. Baughman, J. M. Shacklette, A. A. Zakhidov, and S. Stafström, Nature (London) **392**, 362 (1998).
[65] R. H. Baughman, Nature (London) **425**, 667 (2003).
[66] G. N. Greaves, A. L. Greer, R. S. Lakes, and T. Rouxel, Nat. Mater. **10**, 823 (2011).
[67] R. S. Lakes, Annu. Rev. Mater. Res. **47**, 63 (2017).
[68] J. Dagdelen, J. Montoya, M. de Jong, and K. Persson, Nat. Commun. **8**, 323 (2017).
[69] R. Gaillac, P. Pullumbi, and F.-X. Coudert, J. Phys.: Condens. Matter **28**, 275201 (2016).
[70] A. Marmier, Z. A. Lethbridge, R. I. Walton, C. W. Smith, S. C. Parker, and K. E. Evans, Comput. Phys. Commun. **181**, 2102 (2010).
[71] O. L. Anderson, J. Phys. Chem. Solids **24**, 909 (1963).
[72] O. L. Anderson, E. Schreiber, and N. Soga, *Elastic Constants and Their Measurements* (McGraw-Hill, New York, 1973).
[73] I. Johnston, G. Keeler, R. Rollins, and S. Spicklemire, *Solids State Physics Simulations* (Wiley, New York, 1996).
[74] L. S. Lerner, K. F. Cuff, and L. R. Williams, Rev. Mod. Phys. **40**, 770 (1968).
[75] N. B. Brandt, Y. G. Ponomarev, and S. M. Chudinov, J. Low Temp. Phys. **8**, 369 (1972).
[76] E. Rogacheva, A. Yakovleva, V. Pinegin, and M. Dresselhaus, J. Phys. Chem. Solids **69**, 580 (2008).

[77] R. S. Blewer, N. H. Zebouni, and C. G. Grenier, Phys. Rev. **174**, 700 (1968).
[78] D. C. McCollum and W. A. Taylor, Phys. Rev. **156**, 782 (1967).
[79] H. V. Culbert, Phys. Rev. **157**, 560 (1967).
[80] G. K. White, J. Phys. C **5**, 2731 (1972).
[81] P. Fischer, I. Sosnowska, and M. Szymanski, J. Phys. C **11**, 1043 (1978).
[82] M. Cardona, R. K. Kremer, R. Lauck, G. Siegle, J. Serrano, and A. H. Romero, Phys. Rev. B **76**, 075211 (2007).
[83] R. K. Kremer, M. Cardona, E. Schmitt, J. Blumm, S. K. Estreicher, M. Sanati, M. Bockowski, I. Grzegory, T. Suski, and A. Jezowski, Phys. Rev. B **72**, 075209 (2005).
[84] M. Cardona, R. K. Kremer, R. Lauck, G. Siegle, A. Muñoz, and A. H. Romero, Phys. Rev. B **80**, 195204 (2009).